A&A 493, 1017–1028 (2009)
DOI: 10.1051/0004-6361:200809769

Astronomy & Astrophysics

Formation of interstellar solid CO_2 after energetic processing of icy grain mantles

S. Ioppolo[1,⋆], M. E. Palumbo[1], G. A. Baratta[1], and V. Mennella[2]

[1] INAF – Osservatorio Astrofisico di Catania, via Santa Sofia 78, 95123 Catania, Italy
e-mail: mepalumbo@oact.inaf.it
[2] INAF – Osservatorio Astronomico di Capodimonte, via Moiarello 16, 80131 Napoli, Italy

Received 12 March 2008 / Accepted 26 September 2008

ABSTRACT

Context. Space infrared observations with ISO-SWS and Spitzer telescopes have clearly shown that solid carbon dioxide (CO_2) is ubiquitous and abundant along the line of sight to quiescent clouds and star forming regions. Due to the CO_2 low gas-phase abundance, it is suggested that CO_2 is synthesized on grains after energetic processing of icy mantles and/or surface reactions.
Aims. We study quantitatively the abundance of carbon dioxide synthesized from ice mixtures of astrophysical relevance induced by ion irradiation at low temperature. We compare the CO_2 stretching and bending-mode band profiles observed towards some young stellar objects (YSOs) for which infrared spectra exist.
Methods. Using a high vacuum experimental setup, the effects induced by fast ions (30−200 keV) on several ice mixtures of astrophysical interest are investigated. Chemical and structural modifications of the ice samples that form new molecular species are analyzed using infrared spectroscopy. The formation cross section of solid CO_2 is estimated from the increase in column density as a function of the dose fitting of experimental data with an exponential curve.
Results. Our laboratory experiments showed that carbon dioxide is formed after irradiation of ice mixtures containing C- and O-bearing molecules. Furthermore, when the same amount of energy is released into the icy sample, a larger amount of CO_2 is formed in H_2O-rich mixtures in agreement with previous studies. We also found that the CO_2 stretching and bending mode band profiles depend on the mixture and temperature of the ice sample. We found that the amount of carbon dioxide formed after ion irradiation can account for the observed carbon dioxide towards YSOs. Furthermore, we discovered that laboratory spectra are a good spectroscopic analogue of the interstellar features.
Conclusions. Even if the comparison between laboratory and observed spectra presented here cannot be considered unique and complete, our results quantitatively support the hypothesis that interstellar solid CO_2 forms after ion irradiation and UV photolysis of icy mantles.

Key words. astrochemistry – molecular processes – methods: laboratory – techniques: spectroscopic – ISM: abundances – infrared: ISM

1. Introduction

An unanswered question concerning the astrophysics of the interstellar medium is the origin of solid CO_2 observed along the line of sight to embedded young stellar objects (YSOs) and field stars obscured by dense molecular clouds. Solid CO_2 absorption bands are detected in those regions by the *Infrared Space Observatory* (*ISO*; e.g. Gerakines et al. 1999; Gibb et al. 2004; Nummelin et al. 2001) and by the *Spitzer Space Telescope* (e.g. Boogert et al. 2004; Pontoppidan et al. 2005, 2008; Whittet et al. 2007). Since there is a small abundance of gas phase CO_2 in the interstellar medium, about a factor of 100 less than in the solid state (van Dishoeck et al. 1996; Boonman et al. 2003), which is in agreement with chemical models that predict low CO_2 production efficiency by gas phase reactions (Bergin et al. 1995), it is generally assumed that this molecule is synthesized onto grains. Solid CO_2 could be produced in-situ by means of surface reactions (e.g. Tielens & Hagen 1982; Stantcheva & Herbst 2004; Fraser & van Dishoeck 2004), although this chemical pathway remains controversial. The reaction CO + O → CO_2 was found to have a prohibitively high barrier in at least one study (Grim & d'Hendecourt 1986), while, according to Roser et al. (2001), it proceeds with a small barrier or even barrierless. Extensive laboratory studies of these surface reaction schemes are required. Energetic processing such as UV and ion irradiation of ices containing C- and O-bearing molecules is another possible formation mechanism. Laboratory experiments demonstrated that CO_2 is formed after energetic processing of pure CO ice and icy mixtures containing CO and H_2O (e.g. d'Hendecourt et al. 1986; Moore et al. 1991; Gerakines et al. 1996; Ehrenfreund et al. 1997; Palumbo et al. 1998; Watanabe et al. 2002; Loeffler et al. 2005). Interstellar grains are being continuously exposed to energetic processes such as cosmic ion irradiation and UV photolysis. Fast ions passing through molecular solids release their energy into the target material. As a consequence, many molecular bonds are broken along the ion-track and, in a short time (less than one picosec), and the molecular fragments recombine to produce a rearrangement of the chemical structure that leads to the formation of new molecular species. In the case of UV photolysis, the energy is released into the target material by a single photodissociation or photoexcitation event. In this particular case, new molecular species are also formed (Strazzulla et al. 2001; Palumbo 2005).

⋆ *Present address*: Raymond and Beverly Sackler Laboratory for Astrophysics, Leiden Observatory, Leiden University, PO Box 9513, 2300 RA Leiden, The Netherlands.

Mennella et al. (2004, 2006) suggested that in cold dark clouds, solid CO and CO_2 can be formed by energetic processing of carbon grains with a water ice cap, and they quantitatively evaluated the amount of CO and CO_2 formed. In this scenario, polar CO_2 would be produced mainly on carbon grains when water ice mantles are formed and nonpolar CO_2 would be formed when freeze-out of gas-phase CO takes place. These results represent a different chemical pathway with respect to the grain-surface reaction routes proposed by Bergin et al. (2005). Both mechanisms could contribute to the total solid CO_2 column density detected along the line of sight to dense clouds. Nevertheless, a comprehensive quantitative analysis of the amount of CO_2 formed after irradiation of ice mixtures and a direct comparison with observations is still lacking.

We present results of a quantitative analysis of the CO_2 abundance synthesized by ion irradiation of several ice mixtures at low temperature. In particular, we studied ice mixtures containing carbon monoxide, and ice mixtures that do not contain carbon monoxide but comprise C- and O-bearing molecules. These data and those obtained by Mennella et al. (2004, 2006) are used to fit the CO_2 stretching and bending-mode band profiles observed towards some YSOs. The fits presented here support quantitatively the hypothesis that the formation of interstellar solid CO_2 after energetic processing of icy mantles is an efficient mechanism.

2. Experimental procedure

The experiments are conducted at the Laboratory for Experimental Astrophysics, INAF-Catania Astrophysical Observatory (Italy). A schematic view of the experimental apparatus is shown in Fig. 1. Experiments are carried out in a stainless steel vacuum chamber with base pressure of about 10^{-7} mbar. Inside the vacuum chamber, a crystalline silicon (or KBr) substrate is placed in thermal contact with a cold finger, whose temperature can be varied within the 10–300 K range. A needle valve is used to admit pure gases (or mixtures) into the chamber, where they freeze onto the substrate. Ices are monitored using an FTIR spectrometer (Bruker Equinox 55) at a resolution of 1 cm^{-1}. A He-Ne laser is used to monitor the thickness of the icy film during deposition. The vacuum chamber is connected to an ion implanter (200 kV; Danfysik) from which ions of energy up to 200 keV (400 keV for double ionizations) can be obtained. The ion beam produces a spot on the target larger than the area probed by the IR beam. Current densities range from 100 nA cm^{-2} up to a few μA cm^{-2}. In this set-up, IR spectra can be obtained before and after ion irradiation without tilting the sample. The icy samples studied are deposited and irradiated at 12–16 K. Spectra are acquired before and after irradiation at low temperature and after warm-up at higher temperatures up to 80–90 K. A different procedure is used for only one pure CO deposit. In this case, the sample is grown and is irradiated at 16 K. It is then heated to 70 K and irradiated. It is subsequently cooled to 16 K and irradiated again. This enabled us to study whether the profile of the CO_2 bands changes after further irradiation at higher temperature and after CO sublimation.

At all the examined irradiation doses and temperatures for each sample two spectra, P and S, are taken. With a polarizer placed in the path of the IR beam (Fig. 1), it is possible to select and analyze the P and S component of the IR beam separately. The P polarized component has the electric vector parallel to the plane of incidence (the plane of the figure), while the S polarized component has the electric vector perpendicular to the plane of incidence. The corresponding spectrum of the background acquired before deposition is subtracted from all spectra for a given polarization (Baratta & Palumbo 1998). As shown by Baratta et al. (2000), spectra taken at oblique incidence in S polarization are equivalent to spectra taken at normal incidence.

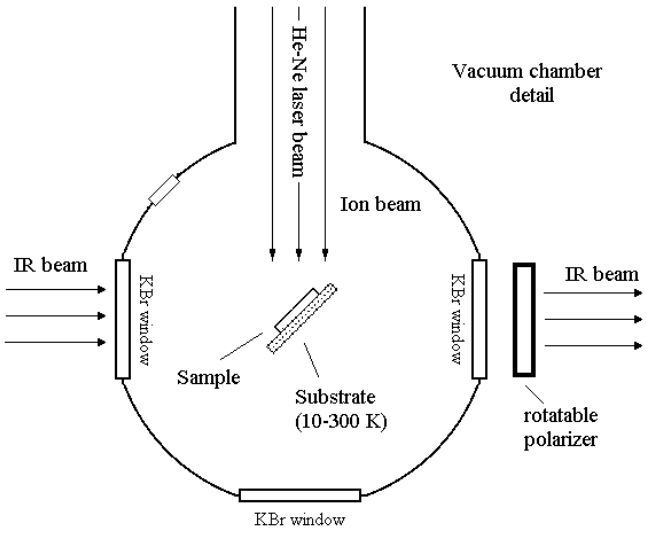

Fig. 1. Schematic top view of the vacuum chamber.

In all examined cases, the penetration depth of impinging ions is larger than the thickness of the sample as verified using the TRIM code (Ziegler 2003). The ions used are H^+ or He^+ at energies of 200 keV and 30 keV, respectively. Results do not depend on the ion used but on the deposited energy, i.e. dose (eV/16 amu), which is calculated from knowledge of the stopping power (energy loss per unit path length) of the ions and measurement of the number of impinging ions per unit of area, fluence (ions cm^{-2}). Some characteristics of the analyzed samples are listed in Table 1. In a few instances, the energy deposited is not uniform throughout the samples. Then the mean stopping power is calculated as $\int S\ \mathrm{d}x / \int \mathrm{d}x$, where $\int \mathrm{d}x$ is the film depth and S is the stopping power calculated by TRIM. The doses are given in eV/16 amu to compare the results of experiments performed with different mixture concentrations and/or using species of different molecular weight.

To estimate the abundance of solid molecules in both laboratory samples and along the line of sight to molecular clouds, it is essential to convert the transmittance spectra (I_f) into optical depth units $\tau(\nu) = \ln(I_o/I_f)$, where I_o is the normalization continuum. We also needed to know the integrated absorbance (cm $molecule^{-1}$) of their IR bands. For the integrated absorbance, we assumed 20×10^{-17} cm mol^{-1} (Allamandola et al. 1988) for the 3 μm H_2O stretching mode, 7.6×10^{-17} cm mol^{-1} (Yamada & Person 1964) for the CO_2 asymmetric stretching mode, 1.1×10^{-17} cm mol^{-1} (Gerakines et al. 1995) for the CO_2 bending mode, 1.1×10^{-17} cm mol^{-1} (Jiang et al. 1975) for the CO stretching mode, 0.64×10^{-17} cm mol^{-1} (Schutte et al. 1993; Mulas et al. 1998) for the C-H deformation mode of CH_4, 1.7×10^{-17} cm mol^{-1} (Lacy et al. 1998) for the umbrella mode of NH_3, and 1.3×10^{-17} cm mol^{-1} (Palumbo et al. 1999) for the C–O stretching mode of CH_3OH. After fitting a straight baseline, the band area $\int \tau(\nu)\mathrm{d}\nu$ is calculated and divided by the integrated absorbance to derive the column density for each considered species.

Table 1. Characteristics of the studied samples. All ice mixtures are irradiated at 12−16 K and then heated to 80−90 K.

Ices	Energy (keV)	Ion	Thickness (nm)	Stopping power (eV/Å)	Dose max (eV/16 amu)
CO	200	H^+	220	6.177	18
CO	200	H^+	990	6.440	32
CO[(a)]	200	H^+	1120	6.585	40
$CO:N_2$ = 8:1	200	H^+	2000	6.800	23
$CO:N_2$ = 1:1	200	H^+	2000	6.900	23
$CO:N_2$ = 1:8	200	H^+	2000	7.100	27
$H_2O:CO$ = 1:10	200	H^+	750	7.311	28
$H_2O:^{13}CO$[(b)] = 6:1	200	H^+	160	9.500	4
$H_2O:CO$ = 8:1	30	He^+	90	8.842	57
$H_2O:CO:N_2$ = 1:3:3	30	He^+	300	7.381	49
$N_2:CH_4:CO$ = 1:1:1	30	He^+	300	8.190	54
$CO:NH_3$ = 2:1	30	He^+	300	7.925	19
CH_3OH	30	He^+	110	10.477	80
$CH_3OH:N_2$ = 1:1	200	H^+	250	9.446	21
$H_2O:CH_4$ = 4:1	30	He^+	90	9.902	180
$H_2O:CH_4$ = 1:1	30	He^+	300	9.078	60
$H_2O:CH_4:N_2$ = 1:1:1	30	He^+	300	8.328	50

[(a)] Sample irradiated at 16 K; heated to 70 K and irradiated; cooled to 16 K and irradiated; [(b)] the $^{13}CO_2$ band is analyzed.

3. Results

3.1. Irradiation of CO bearing mixtures

The formation of solid carbon dioxide is investigated in different mixtures that contain CO ices irradiated at low temperature. All samples considered are listed in Table 2. Among the samples containing CO, pure CO ice is discussed first. The most important product upon irradiation of pure CO ice is solid carbon dioxide. For all samples listed in Table 2, the column density of solid CO_2 (N_{CO_2}) is estimated as a function of irradiation dose:

$$N_{CO_2}/N^0_{CO} = A[1 - e^{-(\sigma_{tot} \times D)}], \quad (1)$$

where $A = A_0/N^0_{CO}$ is the asymptotic value for CO_2 column density (A_0) divided by the initial column density of CO in the sample before the irradiation (N^0_{CO}), σ_{tot} is the total cross section and D is the dose. The best-fit functions fitted to the experimental data are shown in Figs. 2−4, while the values found for A and σ_{tot} are listed in Table 2. It is interesting to note that the column density of CO_2 increases rapidly at low doses and then reaches a saturation value, indicating that a steady state is reached between the formation and destruction mechanisms as discussed by Mennella et al. (2004) and Loeffler et al. (2005). In the case of a pure CO sample, the percentage of CO_2 with respect to the initial CO is in agreement with Loeffler et al. (2005). In the top-left panel of Fig. 2, the results obtained from two different samples of thickness 220 nm and 990 nm are plotted. To evaluate the amount of CO_2 formed by energetic processing, the pure CO sample of thickness 990 nm is fitted with Eq. (1). A larger amount of CO_2 is formed in H_2O-rich mixtures, comparing the results reported in Figs. 2−4, and considering the same amount of energy released to the icy sample, in agreement with previous studies (e.g. d'Hendecourt et al. 1986; Moore et al. 1991; Ehrenfreund et al. 1997; Palumbo et al. 1998; Watanabe et al. 2002). Figure 3, furthermore, plots the results obtained from four mixtures containing CO and H_2O in different proportions. CO_2 molecules formed after ion irradiation in the $H_2O:CO$ = 1:10 mixture represent ∼12% of the initial CO and this value is close to the percentage obtained after irradiation of pure CO, while the column density of CO_2 in a $H_2O:CO$ = 8:1 mixture is about 60% of the initial CO. In the case of the $H_2O:^{13}CO$ = 6:1 mixture, the fit of experimental data provides higher A value (0.92) than in the other considered cases. We note that this is unrealistic. The experimental data points are far from the saturation value and follow an almost linear trend, since irradiation is halted after a dose of ∼4 eV/16 amu, which is lower than those used for the other considered samples. After a dose of ∼30 eV/16 amu, the CO_2 column density in the $H_2O:CO:N_2$ = 1:3:3 mixture decreases because CO_2 molecules, like other species (Baratta et al. 2002), are destroyed after their formation by ion irradiation. We therefore decided to fit the data up till the dose of ∼20 eV/16 amu, which corresponds to the maximum CO_2 formation level reached in this experiment.

Table 2. Best-fit parameters for Eq. (1) to the experimental data regarding samples containing CO ice.

Ices	A[(a)]	σ_{tot}[(b)] (16 amu/eV)
CO[(c)]	0.074 ± 0.002	0.242 ± 0.009
$CO:N_2$ = 8:1	0.092 ± 0.002	0.106 ± 0.005
$CO:N_2$ = 1:1	0.162 ± 0.002	0.090 ± 0.002
$CO:N_2$ = 1:8	0.108 ± 0.004	0.203 ± 0.027
$H_2O:CO$ = 1:10	0.121 ± 0.003	0.125 ± 0.009
$H_2O:^{13}CO$ = 6:1	0.922 ± 0.128	0.107 ± 0.018
$H_2O:CO$ = 8:1	0.567 ± 0.016	0.103 ± 0.013
$H_2O:CO:N_2$ = 1:3:3	0.246 ± 0.004	0.198 ± 0.009
$N_2:CH_4:CO$ = 1:1:1	0.072 ± 0.001	0.105 ± 0.005
$CO:NH_3$ = 2:1	0.131 ± 0.005	0.094 ± 0.007

[(a)] The asymptotic value for CO_2 column density divided by the initial column density of CO before the irradiation; [(b)] the total cross section; [(c)] sample with a thickness of 990 nm (see Table 1).

3.2. Irradiation of ice mixtures without CO

Solid CO and CO_2 are the foremost molecules formed at low temperature after processing of C- and O-bearing ices, which do not contain CO ice initially.

The effects of ion irradiation in a sample of pure solid CH_3OH and in a mixture of H_2O and CH_4 with a ratio 4:1 are quantified. Notice that it is impossible to reproduce the trend of

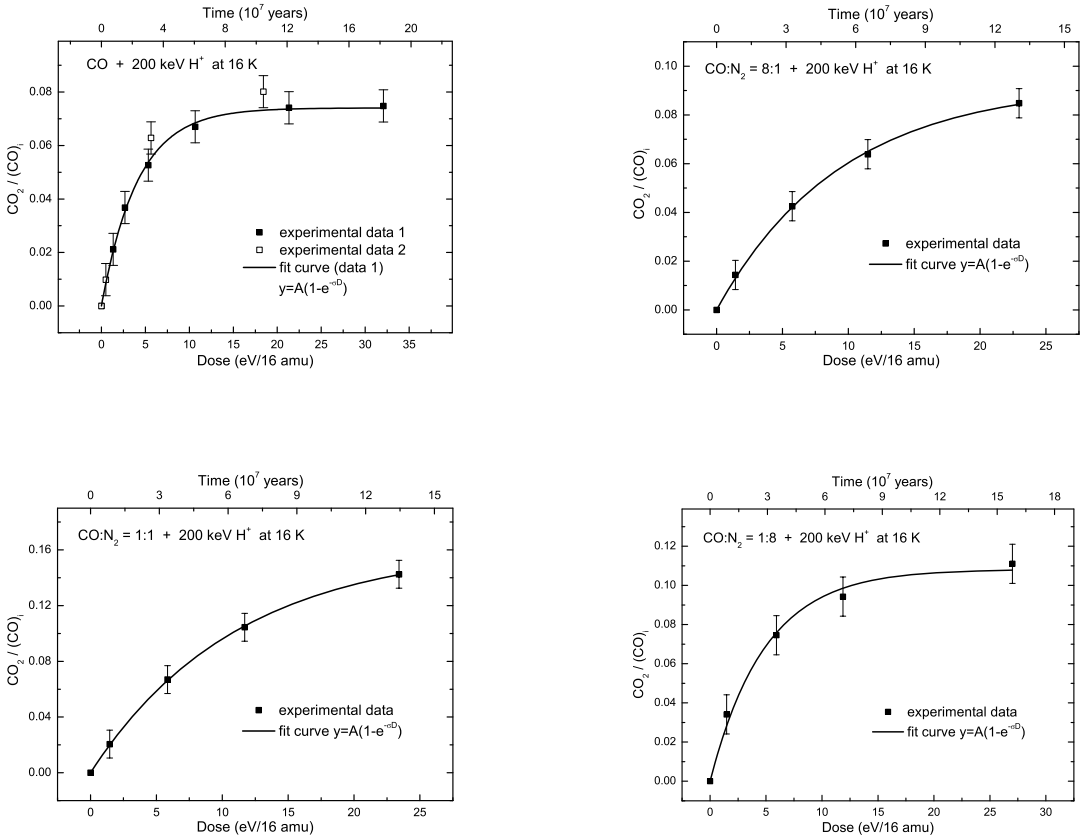

Fig. 2. Column density of CO_2 divided by the initial column density of CO before irradiation for pure CO ice and CO:N_2 mixtures. The column density ratio is plotted as a function of dose. The dose is transferred to interstellar timescales as indicated on *the top x*-axis. Experimental data are fitted to an exponential curve (Eq. (1)): $y = A[1 - e^{-(\sigma D)}]$, where A is the asymptotic value for CO_2 column density divided by the initial column density of CO, σ is the total cross section, and D is the dose. Only the points indicated by data 1 (990 nm thick sample) are used for the fit in the top-left panel. Data 2 (220 nm thick sample) is plotted for comparison.

the CO and CO_2 column density with one exponential curve. For both of the aforementioned mixtures, the experimental column densities of formed CO and CO_2 divided by the initial column densities of CH_3OH and CH_4, respectively, are fitted by two exponential curves with a threshold dose (D_0) to take into account the change in the CO and CO_2 production rate. In the case of CO_2 and for $D \leq D_0$:

$$N_{CO_2}/N_X^0 = A_1[1 - e^{-(\sigma_{tot}^1 \times D)}], \quad (2)$$

while for $D > D_0$:

$$N_{CO_2}/N_X^0 = A_1[1 - e^{-(\sigma_{tot}^1 \times D)}] + A_2[1 - e^{-[\sigma_{tot}^2 \times (D - D_0)]}], \quad (3)$$

where A_1 and A_2 are the asymptotic values of CO_2 column density divided by the initial column density of CH_3OH and CH_4 (N_X^0), for the deposit of pure solid CH_3OH, and, for the 4:1 mixture of H_2O and CH_4 respectively, σ_{tot}^1 and σ_{tot}^2 are the total cross sections, D is the dose and D_0 is the threshold dose. Equations (2) and (3) are also used to quantify the CO column density obtained in both of the aforementioned mixtures by energetic processing at low temperature. The best-fits to experimental data for CO and CO_2 column density divided by N_X^0 as a function of the dose are shown in Fig. 5, while the asymptotic values of CO and CO_2 column density divided by N_X^0 and the total cross sections are listed in Tables 3 and 4 respectively.

During irradiation, the column density of methanol, water, and methane decreases, while the column density of newly formed species, such as CO, CO_2, and H_2CO, increases. We note that at low doses the trend of CO and CO_2 production differs from that at higher doses. Furthermore, at low doses, the main molecules formed are hydrocarbons (Baratta et al. 2002), whose column density decreases at higher doses as the CO and CO_2 column densities increase. First and second generation molecules therefore exist. The presence of newly formed solid CO in the mixture supports the CO_2 synthesis, because reactions with CO as a precursor, such as CO + OH, must be important. In addition, CO_2 could be formed by reactions that do not have CO as a precursor.

3.3. Carbon grains with a water ice cap

According to observations, the ratio of solid CO_2 to H_2O abundance is almost constant (varying from 15% to 40%) toward field stars as well as embedded objects, while the abundance of solid CO with respect to water ice is strongly cloud-density dependent (e.g. Gerakines et al. 1999; Whittet et al. 1998; Nummenin et al. 2001; Bergin et al. 2005; Pontoppidan et al. 2008). This suggests that solid water and carbon dioxide may be formed under similar conditions. During the continuous cycling of dust between diffuse and dense regions in the interstellar medium, an

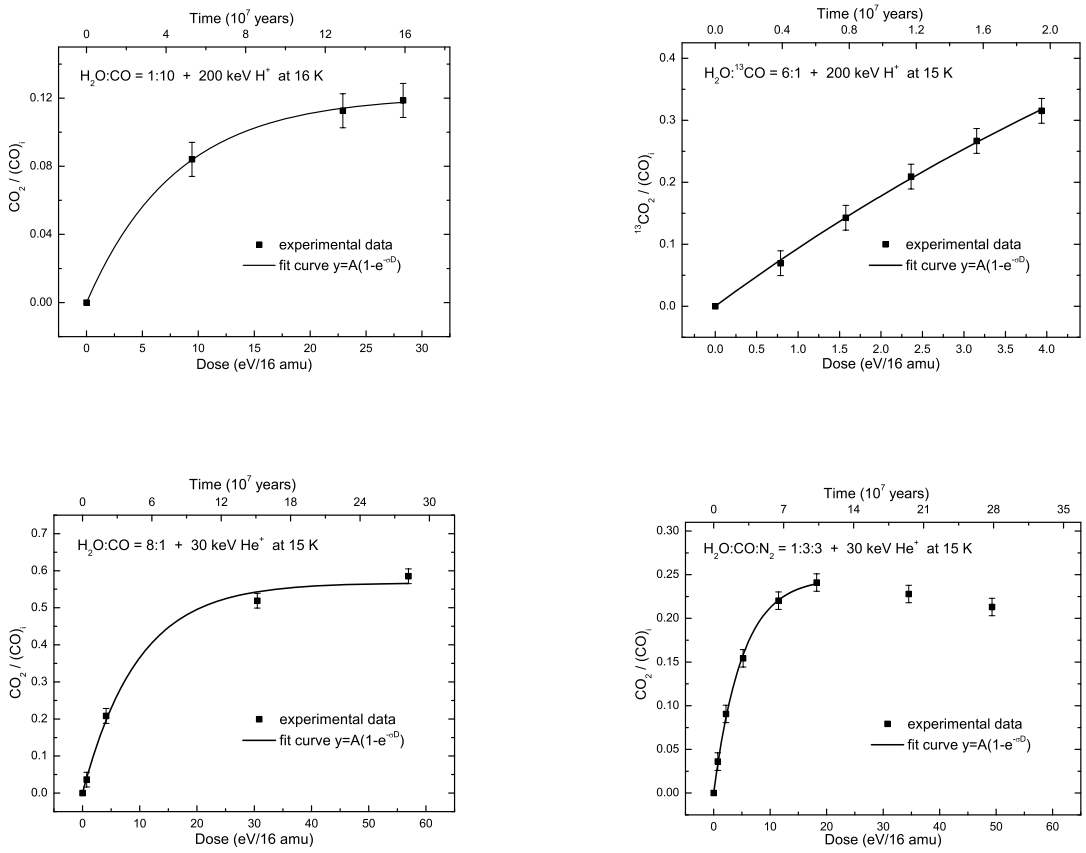

Fig. 3. Column density of CO_2 divided by the initial column density of CO before irradiation for H_2O:CO = 1:10, H_2O:^{13}CO = 6:1, H_2O:CO = 8:1, and H_2O:CO:N_2 = 1:3:3 ice mixtures. The column density ratio is plotted as a function of dose. The dose is transferred to interstellar timescales as indicated on the top *x*-axis. Experimental data are fitted to an exponential curve (Eq. (1)): $y = A[1 - e^{-(\sigma D)}]$, where A is the asymptotic value for CO_2 column density divided by the initial column density of CO, σ is the total cross section, and D is the dose.

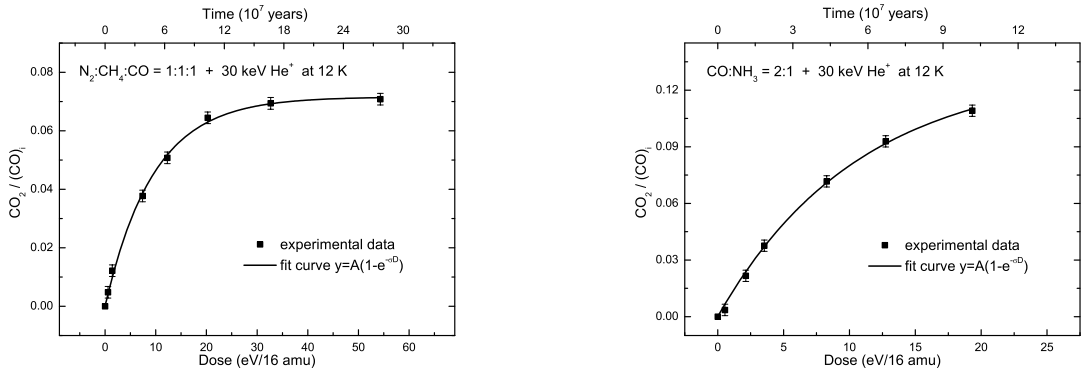

Fig. 4. Column density of CO_2 divided by the initial column density of CO before irradiation for N_2O:CH_4:CO = 1:1:1 and CO:NH_3 = 2:1 ice mixtures. The column density ratio is plotted as a function of dose. The dose is transferred to interstellar timescales as indicated on *the top x*-axis. Experimental data are fitted to an exponential curve (Eq. (1)): $y = A[1 - e^{-(\sigma D)}]$, where A is the asymptotic value for CO_2 column density divided by the initial column density of CO, σ is the total cross section, and D is the dose.

H_2O-rich ice layer covers hydrogenated carbon grains as they enter in dense clouds. A standard cosmic-ray field and UV field induced by cosmic-ray fluorescence of molecular hydrogen can process carbon grains covered by mantles of water ice, leading to the formation of new solid species. Laboratory studies show that formation of CO and CO_2 molecules occurs when hydrogenated carbon grains with a water ice cap are irradiated at low temperature. The experimental results for ion irradiation and UV photolysis of H_2O ice covered carbon grains are described by Mennella et al. (2004, 2006) and represent an alternative efficient formation route with respect to that proposed by Bergin et al. (2005). Nevertheless, we emphasize that both energetic processing and

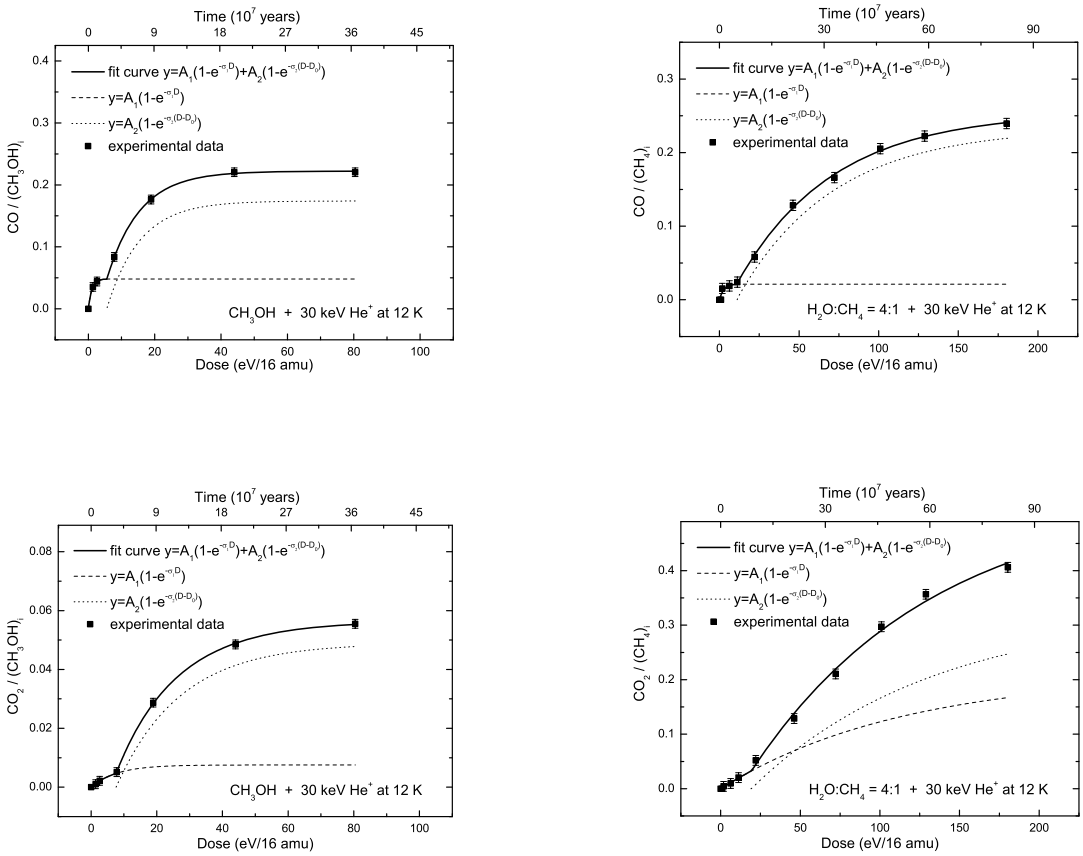

Fig. 5. Column density of CO and CO_2 divided by the initial column density of CH_3OH and CH_4 for the deposit of pure CH_3OH ice and of H_2O:CH_4 = 4:1 mixture, respectively. CO and CO_2 are formed after ion irradiation of icy samples containing C- and O-bearing molecules. The column density ratios are plotted as a function of dose. The dose is transferred to interstellar timescales as indicated on the top *x*-axis. Experimental data are fitted to two exponential curves with a threshold dose (Eqs. (2) and (3)). For $D \leq D_0$: $y = A_1[1 - e^{-(\sigma_1 \times D)}]$, while for $D > D_0$: $y = A_1[1 - e^{-(\sigma_1 \times D)}] + A_2[1 - e^{-[\sigma_2 \times (D - D_0)]}]$, where A_1 and A_2 are the asymptotic values for CO and CO_2 column density divided by the initial column density of CH_3OH and CH_4, σ_1 and σ_2 are the total cross sections, D is the dose, and D_0 is the threshold dose.

Table 3. Best-fit parameters for Eqs. (2) and (3) to the experimental CO column density regarding samples without CO.

Ices	D_0(CO)$^{(a)}$ (eV/16 amu)	A_1(CO)$^{(b)}$	σ^1_{tot}(CO)$^{(c)}$ (16 amu/eV)	A_2(CO)$^{(b)}$	σ^2_{tot}(CO)$^{(c)}$ (16 amu/eV)
CH_3OH	5.5 ± 0.3	0.048 ± 0.004	0.150 ± 0.150	0.174 ± 0.004	0.101 ± 0.004
H_2O:CH_4 = 4:1	10.8 ± 2.9	0.021 ± 0.011	0.376 ± 0.376	0.233 ± 0.013	0.017 ± 0.002

$^{(a)}$ The threshold dose for the exponential curves; $^{(b)}$ the asymptotic values for CO column density divided by the initial column density of CH_3OH and CH_4 before irradiation; $^{(c)}$ the total cross sections.

Table 4. Best-fit parameters for Eqs. (2) and (3) to the experimental CO_2 column density regarding samples without CO.

Ices	D_0(CO_2)$^{(a)}$ (eV/16 amu)	A_1(CO_2)$^{(b)}$	σ^1_{tot}(CO_2)$^{(c)}$ (16 amu/eV)	A_2(CO_2)$^{(b)}$	σ^2_{tot}(CO_2)$^{(c)}$ (16 amu/eV)
CH_3OH	7.6 ± 1.1	0.008 ± 0.006	0.126 ± 0.126	0.049 ± 0.006	0.051 ± 0.007
H_2O:CH_4 = 4:1	19.2 ± 3.0	0.211 ± 0.033	0.009 ± 0.002	0.327 ± 0.033	0.009 ± 0.001

$^{(a)}$ The threshold dose for the exponential curves; $^{(b)}$ the asymptotic values for CO_2 column density divided by the initial column density of CH_3OH and CH_4 before irradiation; $^{(c)}$ the total cross sections.

surface reactions are not mutually exclusive and could rather contribute to the total solid CO_2 observed along the line of sight to dense clouds.

Mennella et al. (2004, 2006) derived the formation cross section of CO and CO_2 molecules from the increase in intensity of the CO and CO_2 stretching modes as a function of the ion and UV fluences, and estimated that after $t = 3 \times 10^7$ yr, column densities are:

$$N_{CO} = 7.0 \times 10^{15} A_V, \quad (4)$$

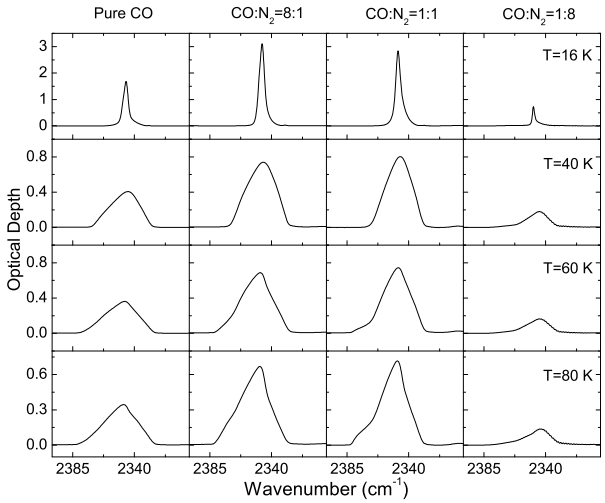

Fig. 6. The band profile of the CO_2 stretching mode at about 2340 cm^{-1} formed after ion irradiation of four different mixtures: (*from the left to the right side*) pure CO ice, $CO:N_2$ = 8:1, $CO:N_2$ = 1:1, and $CO:N_2$ = 1:8. *The top side* of the figure shows the spectrum taken for each experiment after ion irradiation at 16 K. The following rows show the spectra taken after irradiation at 16 K and heated at 40, 60, and 80 K, respectively.

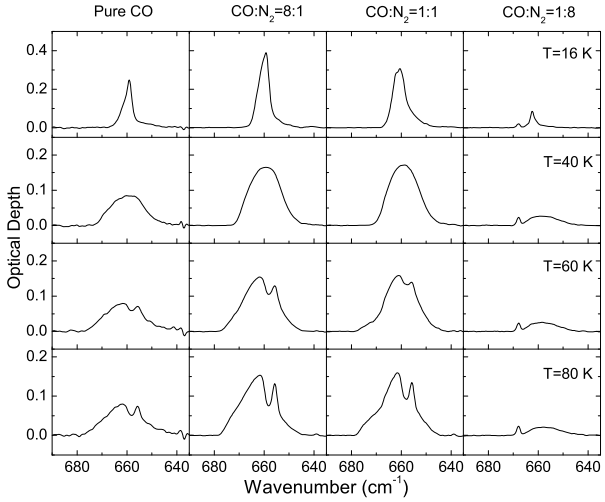

Fig. 7. Similar to Fig. 6 for the CO_2 bending mode at about 660 cm^{-1}.

and

$$N_{CO_2} = 9.3 \times 10^{15} A_V, \quad (5)$$

where A_V is the visual extinction of the cloud.

These laboratory data will be added to our sample and discussed in the following sections.

3.4. Band profiles

In Figs. 6 and 7, we present the band profile of the CO_2 stretching and bending mode (at about 2340 cm^{-1} and 660 cm^{-1} respectively) formed after ion irradiation of four different mixtures. From the left hand side to the right hand side of Figs. 6 and 7, the case of pure CO ice, $CO:N_2$ = 8:1, $CO:N_2$ = 1:1, and $CO:N_2$ = 1:8 are shown. From top to bottom of Figs. 6 and 7, the spectra taken at 16, 40, 60, and 80 K for each experiment, after irradiation at 16 K, are shown. Comparing the band profile of the CO_2 stretching mode for the spectra taken at 16 K with those

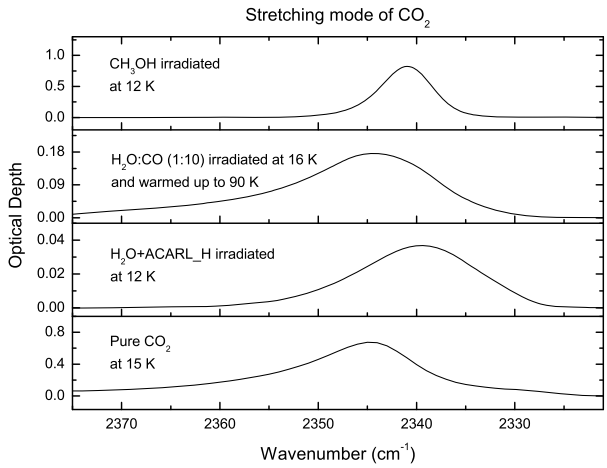

Fig. 8. The band profile of the CO_2 stretching mode at about 2340 cm^{-1} formed after energetic processing at low temperature of some samples: (*from top to bottom*) CH_3OH ice irradiated at 12 K, $H_2O:CO$ = 1:10 irradiated at 16 K and heated to 90 K, water ice deposited on hydrogenated amorphous carbon grains ACARL_H (Mennella et al. 2006) and irradiated at 12 K. The band profile of the stretching mode of pure CO_2 ice at 15 K is also shown for comparison.

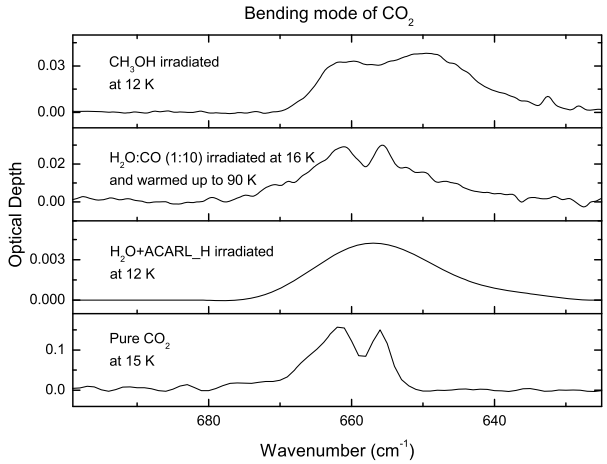

Fig. 9. Similar to Fig. 8 for the CO_2 bending mode at about 660 cm^{-1}.

taken at 80 K it becomes apparent that, after heating the sample, the feature becomes broad and asymmetric. Some differences in peak positions and band widths can also be discerned by comparing the spectra of different samples taken at the same temperature. The bending mode appears more sensitive to temperature variations than the stretching mode. If the sample is heated, the bending mode feature changes drastically: a double peak appears at about 655 cm^{-1} and 660 cm^{-1} and the band becomes broader. The double peak shifts in position and changes in intensity for different N_2 abundance in the mixtures, until it effectively disappears in the spectra for the $CO:N_2$ = 1:8 mixture. At all the investigated temperatures, the spectra of the $CO:N_2$ = 1:8 sample present a peak due to the KBr substrate at about 670 cm^{-1}. The infrared spectra show that, due to the different volatility, after irradiation, CO sublimes at about 30 K, while CO_2 remains in the solid phase up to about 90 K. The band profile of the CO_2 bending mode also depends on the N_2 concentration. In general, the results presented here agree with the study of the CO_2 band profile by Ehrenfreund et al. (1997).

Figures 8 and 9 show the band profile of the CO_2 stretching and bending mode formed after energetic processing at low

Table 5. Young infrared source parameters: distance (d), luminosity (l), visual extinction (A_V), and cold component of CO column density detected in gas phase along the line of sight to some YSOs ($N_{gas(cold)}CO$), solid CO_2 column density observed along the line of sight to some YSOs ($N_{solid}CO_2$).

Sources	d (kpc)	l ($L_\odot$)	A_V (mag)	$N_{gas(cold)}CO$ (10^{19} mol cm^{-2})	$N_{solid}CO_2$ (10^{17} mol cm^{-2})	reference
S140 IRS 1	0.9	2000	23	0.45	4.2(0.1)	1, 4
AFGL 2136	2	7×10^4	94	1.08	7.8(0.3)	1, 3
NGC 7538 IRS 9	2.7	4×10^4	84	1.44	16.3(1.8)	1, 2, 3
NGC 7538 IRS 1	2.8	1.3×10^5	119	1.30	5.1(0.2)	1, 4
W33A	4	1.1×10^5	150	1.96	14.5(1.3)	1, 3

(1) Gibb et al. (2004); (2) Chiar et al. (1998); (3) Tielens et al. (1991); (4) Mitchell et al. (1990).

temperature of other samples. From top to bottom of Figs. 8 and 9, we present the spectrum of CH_3OH ice irradiated at 16 K, a mixture of H_2O:CO = 1:10 irradiated at 16 K and heated to 90 K, and irradiated water ice deposited on hydrogenated amorphous carbon grains called ACARL_H (Mennella et al. 2006). The stretching and bending mode band profiles of pure CO_2 ice are also shown for comparison. It is interesting to note that, although the peak position changes in each spectrum for both the stretching and bending modes, the bending mode appears more sensitive to mixture variations.

4. Comparison with observations

4.1. CO_2 towards massive YSOs

Along the line of sight to embedded young stellar objects (YSO), icy mantles could have been exposed to energetic processing and warming. The observed band profiles due to solid CO_2 indicate the presence of different components along the line of sight. We considered the following YSOs: S140 IRS 1, AFGL 2136, NGC 7538 IRS 9, NGC 7538 IRS 1, and W33A (Gerakines et al. 1999). A list of the considered young infrared source parameters is reported in Table 5.

S140 is an H II region of both high and low mass star formation located 0.9 kpc behind about 23 mag of visual extinction. AFGL 2136 is associated with a bipolar reflection nebula. Along most of the line of sight to AFGL 2136, the dust and the gas temperature is about 30 K. NGC 7538 IRS 9 is an embedded, luminous, and compact infrared source. NGC 7538 IRS 1 is a pre-main-sequence object, which is the most luminous in the NGC 7538 complex. W33A is a massive, luminous source. Along the line of sight to this source, there is evidence for energetic processing provided by the presence of abundant XCN (Gibb & Whittet 2002). In all the considered sources water, carbon monoxide, carbon dioxide and methanol are detected in the solid phase (Gibb et al. 2004).

4.2. The fitting procedure

Gerakines et al. (1999) considered three categories of laboratory mixtures in attempting to reproduce qualitatively the CO_2 stretching and bending mode of the observed, aforementioned spectral features: polar, nonpolar, and annealed ices. In the cases of polar and nonpolar ices, they applied particle shape corrections to the laboratory data using different grain models derived from the real and imaginary parts of the ice's refractive index (n and k values).

In this paper, we have attempted to analyze quantitatively the formation of CO_2 in dense clouds. We have therefore compared the band profiles of CO_2 stretching and bending mode, observed towards embedded YSOs, with laboratory spectra of selected ion-irradiated samples, to assess the effect of energetic processing on interstellar icy mantles.

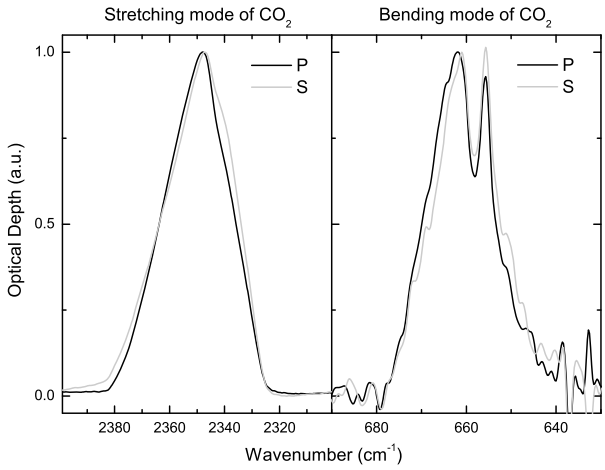

Fig. 10. The band profile of the CO_2 stretching and bending modes formed after irradiation at 16 K and heating to 80 K of pure CO ice. The comparison between the P (*black line*) and S (*light gray line*) component of the IR beam is plotted, see text in Sect. 2.

According to Baratta et al. (2000, 2002), the P polarized component of the spectrum can show additional features that are not due to absorption (k) but to the increased reflectivity of the region across the absorption band where $n < 1$. The difference between the P and S polarized components of the spectra depends on the optical constants of the ice. Additionally, for a given sample, it depends on the thickness, being higher for thinner films. Baratta et al. (2000) also demonstrated that if P and S polarized components differ, then band profiles are unrepresentative of small particle extinction spectra and cannot be compared with observed interstellar spectra. Figure 10 shows the band profile of the stretching and bending mode for CO_2 formed after irradiation of the CO ice, indicating that the P and S components are similar. We verified that this is true for all band profiles used in the fits. Given that the signal-to-noise ratio of P spectra is higher than for S spectra, the former are used to fit the observed data. Since P and S spectra are similar, small particle extinction cross section calculations are in our case unnecessary. For this reason, we used the laboratory spectra in optical depth units for the fitting procedure.

Looking at the observed interstellar spectra, the 4.27 μm feature due to the CO_2 stretching mode is clearly saturated for NGC 7538 IRS 9 and W33A (Fig. 11). AFGL 2136 exhibits a shallow shoulder on the long wavelength side of the 4.27 μm feature. It is suspected that this is the result of an unidentified,

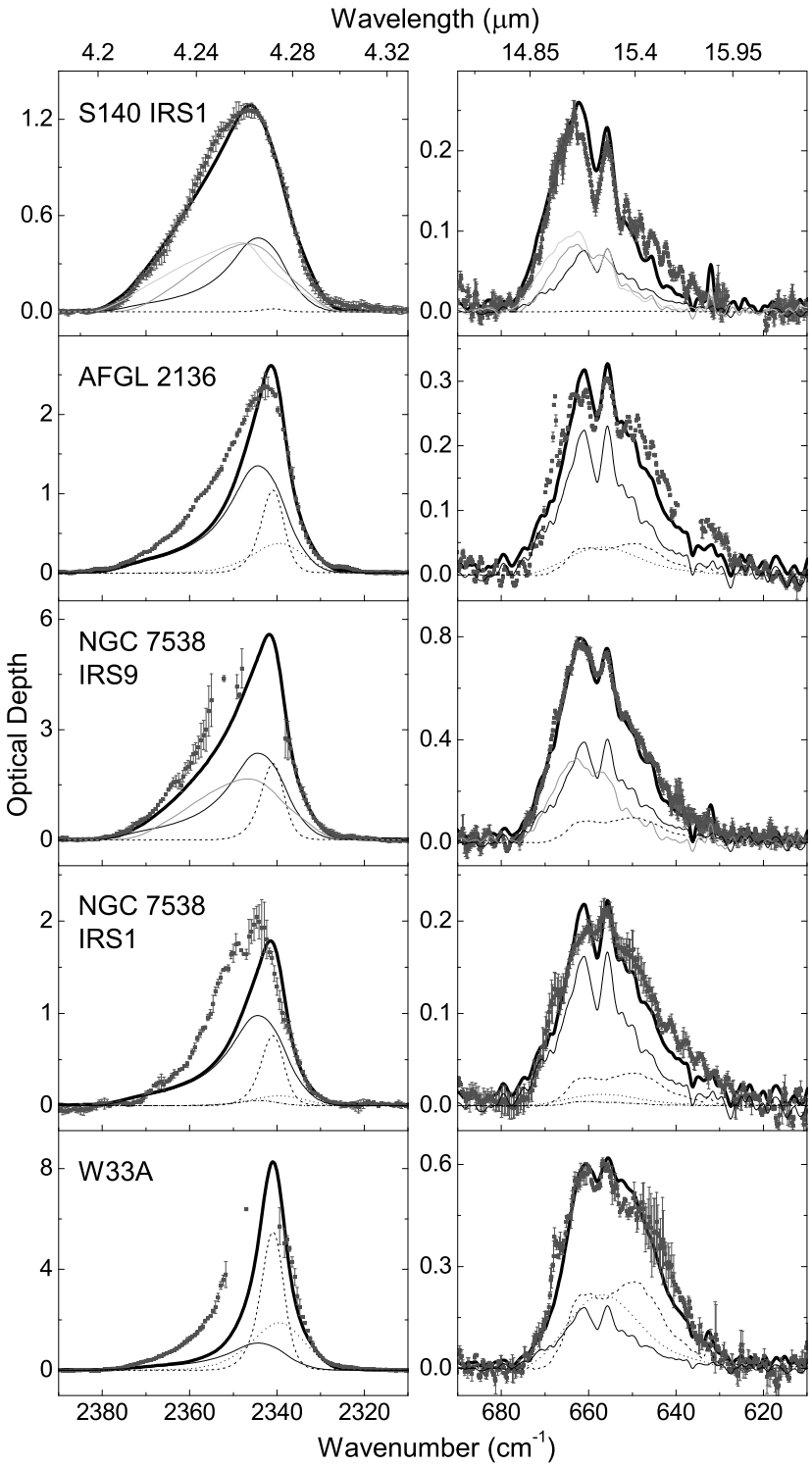

Fig. 11. The CO_2 stretching and bending mode band profile of selected YSO sources are fitted (thick black line) at the same time using different laboratory spectra: CO ice irradiated at 16 K, heated to 70 K and irradiated (light gray line); CO ice irradiated at 16 K, heated to 70 K and irradiated, cooled to 16 K and irradiated (gray line); H_2O:CO = 1:10 mixture irradiated at 16 K and heated to 90 K (black line); CO:NH_3 = 2:1 irradiated at 12 K (dash-dot line); methanol ice irradiated at 12 K (dash line); water ice on hydrogenated carbon grains irradiated at 12 K (dot line). The spectra used to fit the observed CO_2 band profiles are available in the Catania database (http://www.oact.inaf.it/weblab/).

broad, underlying component (Gerakines et al. 1999). The shallow absorption shoulders on the short and long wavelength sides of the stretching mode are due to the unresolved P and R branches of gas-phase CO_2, which are consistent with the strong gas-phase CO_2 absorptions detected at 14.97 μm toward these sources. Spurious structures also exist in the troughs of the 4.27 μm feature of NGC 7538 IRS 1, which may be close to saturation. The observed CO_2 15.2 μm bending mode for all the sources can be divided into three components: a feature at 14.97 μm due to gas-phase CO_2 absorption, a pair of sharp peaks at about 15.15 and 15.27 μm that highlight CO_2 segregation induced by thermal processing along the line of sight, and a

shoulder close to 15.4 μm assigned to the acid-base interaction between CO_2 and alcohols (Ehrenfreund et al. 1998; Dartois et al. 1999).

Using home-written software, all spectra for samples listed in Table 1 are compared systematically with the observed YSOs data. The software selected spectra of laboratory mixtures that fitted simultaneously the CO_2 bending and stretching mode band profile of the source considered. The best results are reported in Fig. 11.

We note that three or four components are needed to fit simultaneously the bending and stretching mode band profile of each object. The fit components and percentages are shown in Table 6. The spectra used to fit the observed CO_2 band profiles are available in the Catania database (http://www.oact.inaf.it/weblab/).

The profile of CO_2 formed after irradiation of a pure CO or a H_2O:CO = 1:10 mixture heated to 70 K is required to reproduce the sharp peaks of the bending mode profile at 15.15 and 15.27 μm. The profile of CO_2 formed after irradiation of methanol is required to fit the shoulder at 15.4 μm. This component is due to an acid-base interaction between the C atom of CO_2 and the oxygen atom of a polar molecule. When CO_2 molecules are in the presence of alcohol, they act as a Lewis acid (Ehrenfreund et al. 1998; Dartois et al. 1999). The most abundant alcohol detected in dense clouds is methanol. For this reason, we considered a sample of methanol deposited and irradiated at low temperature. The profile of CO_2 bending and stretching modes formed after irradiation of H_2O on carbon grains are broad and smooth (Figs. 8 and 9), and these are also required to fit the observed bands.

In the case of NGC 7538 IRS 1, the fit improves if we consider a small contribution (2%) from CO_2 formed after irradiation of a CO:NH_3 = 2:1 mixture. An upper limit to the abundance of ammonia ($<3.7 \times 10^{17}$ cm^{-2}) is indeed derived along the line of sight to NGC 7538 IRS 1 (Gibb et al. 2001).

Finally, it is noted that the considered sample of laboratory spectra is by no means complete and should be regarded only as a starting point for the analysis of the composition of the icy grain mantles. Future studies of the composition of the CO_2 ices should include other laboratory samples of a range of ion and UV irradiation doses, temperatures, and mixture ratios.

From Fig. 11, it is clear that while the bending mode profile is always well reproduced by laboratory spectra, the fit of the stretching mode is not always satisfactory. This could be due to the fact that the optical depth of the stretching mode band is very large and our approach could be no longer applicable.

Pontoppidan et al. (2008) performed a fitting analysis of the CO_2 ice bending mode profile for a large sample of low mass embedded young stars. They used five components to reproduce the profile of the considered feature. A CO_2:H_2O ~ 1:7 mixture and a CO_2:CO ~ 1:1 mixture, which are named the red and blue component respectively, generally dominate the bending mode profile and the total CO_2 column density observed. The other three components are needed to reproduce subtle differences due to trace constituents. All components considered by Pontoppidan et al. (2008) correspond to interstellar relevant ice analogues and can be divided into polar and nonpolar ices. Our fitting results presented here are similar to those of Pontoppidan et al. (2008), although we emphasize that our fitting components are obtained after energetic processing of interstellar ice analogues and both stretching and bending modes are fitted simultaneously without any particle-shape correction.

5. Discussion

Deriving a reliable fit is insufficient to prove the validity of a model; reasonable physical arguments are also required. We have performed a quantitative study of the CO_2 formed in laboratory C- and O-bearing samples upon energetic processing, and we extended our results to the interstellar medium by considering the lifetime in solid phase of species irradiated in dense cores, and the temperature gradient along the line of sight.

In Figs. 2–5 the top ordinate axes indicate an estimation of the time (years) required to achieve the same effect on interstellar ices as observed in the laboratory. To estimate this time, we considered the approximation of effective monoenergetic 1 MeV protons assuming that in dense interstellar regions the effective 1 MeV proton flux is equal to 1 proton cm^{-2} s^{-1} (Mennella et al. 2003). The laboratory results are extrapolated to the interstellar medium conditions by deriving the formation cross section due to 1 MeV protons from that obtained in the irradiation experiments with 30 keV He^+ and 200 keV H^+ using the ratio of the corresponding stopping power as a scaling factor.

As reported by Greenberg (1982), a dense cloud lifetime ranges between 3×10^7 and 5×10^8 yr. Assuming a density of $n_0 \sim 10^4$ cm^{-3}, the gas takes $10^9/n_0 \simeq 10^5$ yr to condense onto grains (Tielens & Allamandola 1987). Icy grain mantles therefore undergo cosmic ion irradiation for about 10^5–10^8 yr. The first estimate refers to the case of icy mantles that sublime as soon as they form (which could be the case for volatile species such as CO), the latter estimate refers to the limit case of icy mantles that survive throughout the cloud lifetime (which could be the case for less volatile species such as H_2O). The lifetime of molecules in the solid phase is related to the volatility of each species. The results of the fits discussed in Sect. 4 and summarized in Table 6, indicate that a significant percentage of the CO_2 band profiles is reproduced by the spectra of CO_2 formed after ion irradiation of pure CO or H_2O:CO = 1:10 ice mixtures. To justify this result, we should assume that all the CO molecules that we observe today in the gas phase along the line of sight to YSOs are frozen onto grains during the cloud collapse phase and have been processed by ion irradiation for about 8×10^6 yr. Then, as indicated by laboratory experiments, when the temperature of the grains increases, CO molecules sublimate, while CO_2 molecules formed after ion irradiation remain. Thus, the profile of the bending mode shows the pair of sharp peaks required to fit the observed band profile. To estimate the amount of solid CO_2 that can form after ion irradiation of CO-rich icy mantles, we therefore use the following equation:

$$N_{CO_2} = N(CO)_{Obs,gas} \times [N(CO_2)/N(CO)]_{Lab,\ solid}, \quad (6)$$

where $N(CO)_{Obs,\ gas}$ is the CO column density detected in gas phase along the line of sight to the considered sources, while $[N(CO_2)/N(CO)]_{Lab,\ solid}$ is the ratio of the CO_2 to CO column density obtained in laboratory spectra.

Solid CO is also observed along the line of sight to YSOs and we then expect that the spectrum of solid CO_2 at low temperatures, formed after ion irradiation of pure CO, should also be considered in the fit of the CO_2 observed band profile. As already discussed by Loeffler et al. (2005), this component accounts for 1–6% of the observed solid CO_2. We included this component in the fitting procedure and found that the quality of the fit is equivalent to that obtained by considering the mixtures listed in Table 6 and shown in Fig. 11. This result agrees with the result obtained by Pontoppidan et al. (2008), who found that the contribution of the CO_2:CO ~ 1:25 mixture is almost negligible.

Table 6. Contributions in percentage for each listed fit component to the total CO_2 column density observed along the line of sight to the considered sources as obtained from the fitting procedure (Fit columns) and as estimated from Eqs. (5)−(8) which give the maximum possible contribution by each component to the total observed CO_2 (Eq. columns).

Spectra	S140 IRS 1		AFGL 2136		NGC 7538 IRS 9		NGC 7538 IRS 1		W33A		
	Fit (%)	Eq. (%)	Fit (%)	Eq. (%)	Fit (%)	Eq. (%)	Fit (%)	Eq. (%)	Fit (%)	Eq. (%)	[Eq.]
CO[(a)]	38	71	–	–	–	–	–	–	–	–	[6]
CO[(b)]	33	71	–	–	41	59	–	–	–	–	[6]
H_2O:CO[(c)] = 1:10	28	100	66	100	44	100	72	100	23	100	[6]
CO:NH_3[(d)] = 2:1	–	–	–	–	–	–	2	2	–	–	[8]
CH_3OH[(d)]	1	83	19	78	15	43	20	92	44	100	[7]
ACARL_H[(d)]	–	–	15	100	–	–	6	100	33	96	[5]

[(a)] Irradiated at 16 K; heated to 70 K and irradiated; [(b)] irradiated at 16 K; heated to 70 K and irradiated; cooled to 16 K and irradiated; [(c)] irradiated at 16 K and heated to 90 K; [(d)] irradiated at 12 K.

To estimate the amount of solid CO_2 formed after ion irradiation of methanol, we used the following equation:

$$N_{CO_2} = N(CH_3OH)_{Obs,\ solid} \times [N(CO_2)/N(CH_3OH)]_{Lab,\ solid}, \quad (7)$$

where the time considered is the lifetime of the dense cloud (3×10^7 yr), $N(CH_3OH)_{Obs,\ solid}$ is the methanol detected in solid phase along the line of sight to the considered sources, and $[N(CO_2)/N(CH_3OH)]_{Lab,\ solid}$ is the ratio of the CO_2 to CH_3OH column density measured in the laboratory spectrum used for the fit. We point out that this ratio is not the $CO_2/(CH_3OH)_i$ ratio reported in Fig. 5.

To estimate the amount of CO_2 formed after ion irradiation of CO:NH_3 = 2:1 mixture we used the following equation:

$$N_{CO_2} = N(NH_3)_{Obs,\ solid} \times [N(CO_2)/N(NH_3)]_{Lab,\ solid}, \quad (8)$$

where $N(NH_3)_{Obs,\ solid}$ is the column density of NH_3 observed along the line of sight to the sources and $[N(CO_2)/N(NH_3)]_{Lab,\ solid}$ is the CO_2 and NH_3 column density ratio measured in the laboratory spectrum used for the fit. In this calculation, we assumed that all solid ammonia observed along the line of sight is mixed with CO.

Following Mennella et al. (2006), and considering clouds for which visual extinction (A_V) is known, we used Eq. (5) to evaluated the contribution of CO_2, which is produced by energetic irradiation of carbon grains with a water ice cap, to the observed column density.

In Table 6, the percentages of the CO_2 column density calculated by Eqs. (5)−(8) are compared to the percentages obtained by fits for all young infrared sources considered. These percentages indicated by "Eq." represent the maximum possible contribution by each component. It is relevant to note that the percentages for the fit components of each YSOs considered agree with the percentages of the CO_2 column density calculated by Eqs. (5)−(8). In all cases analyzed, the percentage values for the fit components are indeed lower than the values derived from Eqs. (5)−(8). Even though the fits presented here are not unique, they are supported by reasonable astrophysical hypotheses as discussed above.

By assuming that in dense clouds all CO molecules detected in the gas phase (CO_{tot}) are frozen onto grains during the cloud collapse phase, it is possible to evaluate, using Table 7, the contribution, due to irradiation, of pure CO ice to the observed CO_2 column density. For the other ice mixtures listed in Table 7, CO_{in} is the amount of interstellar solid CO originally present in icy grain mantles and mixed with other species. For those lines of sight along which visual extinction are known, it is possible to calculate the contribution to the solid CO_2 due to irradiation of carbon particles covered by amorphous water ice.

Table 7. Contribution of CO_2 produced by energetic irradiation of laboratory samples to the observed column density for those clouds of which the visual extinction and the CO gas-phase abundance are known.

Icy samples	N_{CO_2} (upper limits) (mol cm^{-2})
CO	$0.07 \times CO_{tot}$
CO:N_2 = 8:1	$0.09 \times CO_{in}$
CO:N_2 = 1:1	$0.16 \times CO_{in}$
CO:N_2 = 1:8	$0.11 \times CO_{in}$
H_2O:CO = 1:10	$0.12 \times CO_{in}$
H_2O:CO = 8:1	$0.57 \times CO_{in}$
H_2O:CO:N_2 = 1:3:3	$0.25 \times CO_{in}$
N_2:CH_4:CO = 1:1:1	$0.07 \times CO_{in}$
CO:NH_3 = 2:1	$0.13 \times CO_{in}$
ACARL_H	9.3×10^{15} A_V

6. Conclusions

Abundant amount of solid CO_2 is detected towards embedded YSOs (both low mass and high mass protostars) and field stars. Observations towards high mass star-forming regions indicate that some of the observed carbon dioxide is segregated (Ehrenfreund et al. 1998). On the other hand, observations along the line of sight to field stars indicate that most solid CO_2 is mixed with water ice (Bergin et al. 2005). As shown in this article, CO and CO_2 are formed easily after energetic processing of ice mixtures containing C- and O-bearing molecules and carbon grains covered by water ice. Furthermore, given the same amount of energy released to the icy sample, a larger amount of CO_2 is formed in H_2O-rich mixtures. It has been found that the band profile of the CO_2 stretching and bending modes depends on the mixture and temperature of the ice sample. On the basis of the present laboratory results, it is possible to estimate the contribution of CO_2, produced after energetic processing, to the observed carbon dioxide column densities for several YSOs. Laboratory results presented account not only quantitatively for the column density of observed interstellar CO_2 but also provide a good spectroscopic analogue of the interstellar features supporting the hypothesis that interstellar solid CO_2 is formed after ion irradiation and UV photolysis of icy mantles. This however does not exclude the possibility that other formation routes, such as grain surface reactions, contribute to the production of the observed interstellar solid CO_2.

Acknowledgements. This work is supported by MIUR and INAF research contracts. We thank F. Spinella for his technical assistance during laboratory measurements.

References

Allamandola, L. J., Sandford, S. A., & Valero, G. J. 1988, Icarus, 76, 225
Baratta, G. A., & Palumbo, M. E. 1998, JOSA A, 15, 3076
Baratta, G. A., Palumbo, M. E., & Strazzulla, G. 2000, A&A, 357, 1045
Baratta, G. A., Leto, G., & Palumbo, M. E. 2002, A&A, 384, 343
Bergin, E. A., Langer, W. D., & Goldsmith, P. F. 1995, ApJ, 441, 222
Bergin, E. A., Melnick, G. J., Gerakines, P. A., Neufeld, D. A., & Whittet, D. C. B. 2005, ApJ, 627, L33
Boogert, A. C. A., Pontoppidan, K. M., Lahuis, F., et al. 2004, ApJS, 154, 359
Boonman, A. M. S., van Dishoeck, E. F., Lahuis, F., & Doty, S. D. 2003, A&A, 399, 1063
Chiar, J. E., Gerakines, P. A., Whittet, D. C. B., et al. 1998, ApJ, 498, 716
Dartois, E., Demyk, K., d'Hendecourt, L. B., & Ehrenfreund, P. 1999, A&A, 351, 1066
d'Hendecourt, L. B., Allamandola, L. J., Grim, R. J. A., & Greenberg, J. M. 1986, A&A, 158, 119
Ehrenfreund, P., Boogert, A. C. A., Gerakines, P. A., Tielens, A. G. G. M., & van Dishoeck, E. F. 1997, A&A, 328, 649
Ehrenfreund, P., Dartois, E., Demyk, K., & d'Hendecourt, L. 1998, A&A, 339, L17
Fraser, H. J., & van Dishoeck, E. F. 2004, Adv. Space Res., 33, 14
Frost, M. J., Sharkey, P., & Smith, I. W. M. 1991, Faraday Discuss. Chem. Soc., 91, 305
Gerakines, P. A., Schutte, W. A., Greenberg, J. M., & van Dishoeck, E. F. 1995, A&A, 296, 810
Gerakines, P. A., Schutte, W. A., & Ehrenfreund, P. 1996, A&A, 312, 289
Gerakines, P. A., Whittet, D. C. B., Ehrenfreud, P., et al. 1999, ApJ, 522, 357
Gibb, E. L., & Whittet, D. C. B. 2002, ApJ, 566, 113
Gibb, E. L., Whittet, D. C. B., & Chiar, J. E. 2001, ApJ, 558, 702
Gibb, E. L., Whittet, D. C. B., Boogert, A. C. A., & Tielens, A. G. G. M. 2004, ApJS, 151, 35
Greenberg, M. 1982, in Comets, ed. L. L. Wilkening (Tucson: The University of Arizona Press), 131
Grim, R. J. A., & d'Hendecourt, L. B. 1986, A&A, 167, 161
Jiang, G. P., Person, W. B., & Brown, K. G. 1975, J. Chem. Phys., 64, 1201
Lacy, J. H., Faraji, H., Sandford, S. A., & Allamandola, L. J. 1998, ApJ, 501, L105
Loeffler, M. J., Baratta, G. A., Palumbo, M. E., Strazzulla, G., & Baragiola, R. A. 2005, A&A, 435, 587
Mennella, V., Baratta, G. A., Esposito, A., Ferini, G., & Pendleton, Y. J. 2003, ApJ, 587, 727
Mennella, V., Palumbo, M. E., & Baratta, G. A. 2004, ApJ, 615, 1073
Mennella, V., Baratta, G. A., Palumbo, M. E., & Bergin, E. A. 2006, ApJ, 643, 923
Mitchell, G. F., Maillard, J. P., Allen, M., Beer, R., & Belcourt, K. 1990, ApJ, 363, 554
Moore, M. H., Khanna, R., & Donn, B. 1991, J. Geophys. Res., 96, 17541
Mulas, G., Baratta, G. A., Palumbo, M. E., & Strazzulla, G. 1998, A&A, 333, 1025
Nummelin, A., Whittet, D. C. B., Gibb, E. L., Gerakines, P. A., & Chiar, J. E. 2001, ApJ, 558, 185
Palumbo, M. E. 2005, in Massive Star Birth: A Crossroads of Astrophysics Proceedings IAU Symp., 227, ed. R. Cesaroni, M. Felli, E. Churchwell, & C. M. Walmsley
Palumbo, M. E., Baratta, G. A., Brucato, J. R., et al. 1998, A&A, 334, 247
Palumbo, M. E., Castorina, A. C., & Strazzulla, G. 1999, A&A, 342, 551
Pontoppidan, K. M., Dullemond, C. P., van Dishoeck, E. F., et al. 2005, ApJ, 622, 463
Pontoppidan, K. M., Boogert, A. C. A., Fraser, H. J., et al. 2008, ApJ, 678, 1031
Roser, J. E., Vidali, G., Manicò, G., & Pirronello, V. 2001, ApJ, 555, L61
Sandford, S. A., Allamandola, L. J., Tielens, A. G. G. M., & Valero, G. J. 1988, ApJ, 329, 498
Schutte, W. A., Allamandola, L. J., & Sandford, S. A. 1993, Icarus, 104, 118
Stantcheva, T., & Herbst, E. 2004, A&A, 423, 241
Strazzulla, G., Baratta, G. A., & Palumbo, M. E. 2001, Spectrochem. Acta Part A, 57, 825
Tielens, A. G. G. M., & Hagen, W. 1982, A&A, 114, 245
Tielens, A. G. G. M., & Allamandola, L. J. 1987, in Physical processes in interstellar clouds, ed. G. E. Morfill, & M. Scholer (Dordrecht: Reidel), 333
Tielens, A. G. G. M., Tokunaga, A. T., Geballe, T. R., & Baas, F. 1991, ApJ, 381, 181
van Dishoeck, E. F., Helmich, F. P., de Graauw, T., et al. 1996, A&A, 315, L349
Watanabe, N., & Kouchi, A. 2002, ApJ, 567, 651
Whittet, D. C. B., Gerakines, P. A., Tielens, A. G. G. M., et al. 1998, ApJ, 498, L159
Whittet, D. C. B., Shenoy, S. S., Bergin, E. A., et al. 2007, ApJ, 655, 332
Yamada, H., & Person, W. B. 1964, J. Chem. Phys., 41, 2478
Ziegler, J. F. 2003, Stopping and Range of Ions in Matter SRIM2003 (available at `www.srim.org`)